Contents

1 Introduction

In this experiment, a scanning tunneling microscope (STM) is used to examine the surface of graphite, gold and molybdenum disulfide (MoS2).

First, a platinum iridium tip for the STM is prepared with a wire cutter and a pair of pliers. If a tip with satisfactory resolution is manufactured, it can then be used to scan the surface of the materials mentioned above.

These pictures should be evaluated and used to determine the lattice constant of graphite, as well as illustrate the surface structure of a gold covered micro-grid and the atomic structure of MoS2.

2 Theory

In this section, an overview of the theoretical background necessary for this experiment is given. The imaging method used by the STM as well as the surface structure of the materials to be observed will be discussed.

2.1 Quantum Tunneling

The information in this section is based on [2].

Quantum tunneling is an effect in quantum mechanics. It describes the phenomenon of a particle wave function propagating through a potential barrier with a potential $V_0 > E$, where E is the energy of the particle, for example an electron. This is an effect which breaks with the classical description of mechanics. In classical mechanics, the electron will be reflected. However, quantum mechanics allows for a non-zero probability of transmission.

In quantum mechanics, the state of a physical system is described by its wave function. The time evolution of the system is given by the schrödinger equation

$$i\hbar\frac{\partial\psi}{\partial t} = \hat{H}\psi\,, \tag{1}$$

where ψ is the wave function and $\hat{H}$ is the hamiltonian of the system.

The potential $V(x)$ of a system with a potential barrier is given by

$$V(x) = \begin{cases} 0 & \text{for} \quad x < -\frac{a}{2} \\ V_0 & \text{for} \quad -\frac{a}{2} < x < \frac{a}{2} \\ 0 & \text{for} \quad x > \frac{a}{2}\,. \end{cases} \tag{2}$$

It is illustrated in fig. 1.

The schrödinger equation has to be solved for each of the areas $x < -a/2$, $-a/2 < x < a/2$, and $x > a/2$ (before the potential barrier, in the potential barrier and behind the potential

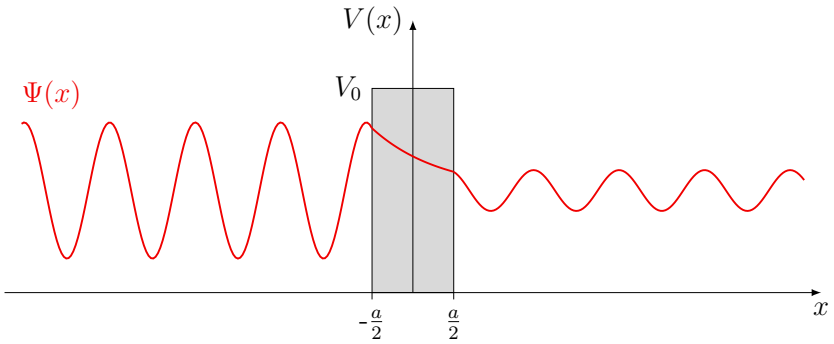

Figure 1: Schematic illustration of quantum tunneling for a particle with an energy of $E < V_0$. The wave function $\Psi(x)$ is shown in red. For $-a/2 < x < a/2$, an exponential decrease of the amplitude can be seen.

barrier). In doing so, the boundary conditions of continuity and differentiability of the electron wave function at $x = -a/2$ and $x = a/2$ have to be met. The solution for the electron wave function is pictured in fig. 1. In the areas $x < -a/2$ and $x > a/2$, the wave function is described by a standing wave. Inside the potential barrier, the electron wave function decreases exponentially.

The probability of the electron passing the barrier is given by

$$P = \exp\left(-\frac{2a}{\hbar}\sqrt{2m\,(V_0 - E)}\right). \tag{3}$$

The tunnel effect can be observed when a voltage U is applied to two conducting materials separated by a potential barrier, e.g. a thin layer of vacuum or air. In this case, a tunneling current I created by electrons tunneling through the gap can be observed. It is proportional to the voltage and the transmission probability given in eq. (3) and exponentially decreases with the gap width a

$$I \propto U \cdot \exp\left(-\frac{2a}{\hbar}\sqrt{2m\,(V_0 - E)}\right). \tag{4}$$

2.2 Band Theory

If not specified otherwise, the information in this subsection is taken from [3].

Solving the schrödinger equation for a single atom leads to discrete electronic energy levels. When several atoms are close to each other, their electrons interact, which slightly shifts the energy levels and splits them up. In a solid body, the number of interacting atoms is very large. This leads to a continuum of possible energy levels, the so-called bands. The bands have different, finite widths, which stem from the overlap of the atomic orbitals. As the band widths are finite, gaps may occur, the so-called band gaps.

Band theory can be used to explain material properties of conductors, semiconductors and isolators. The core bands, corresponding to low electronic energy states, are usually completely filled, while bands at very high energy levels are almost never filled. Therefore, the bands of interest when describing material properties are those located near the Fermi

energy, which is the energy up to which all states are filled at a temperature of 0 K. For higher temperatures, thermal energy leads to some electrons having a higher energy and moving to a higher energy level. Then, some energy levels just below the Fermi energy are not filled, while a few higher ones are.

In an isolator, the Fermi energy is located in a large band gap. All bands are either completely filled or empty. In an external electric field, none of the electrons can move.

In a metal, the Fermi energy is located within a band. At temperatures higher than 0 K, the distribution of the filled energy levels around the Fermi energy allows these electrons to move freely between atoms.

In semiconductors, the Fermi energy is located in a small energy gap. The band located directly below the Fermi energy is called valence band, and the band located directly above the Fermi energy is called conduction band. Thermal fluctuations lead to some electrons being in the conduction band, while some configurations in the valence band are free.

A sketch of the band theory for conductors, semiconductors and isolators can be found in fig. 2.

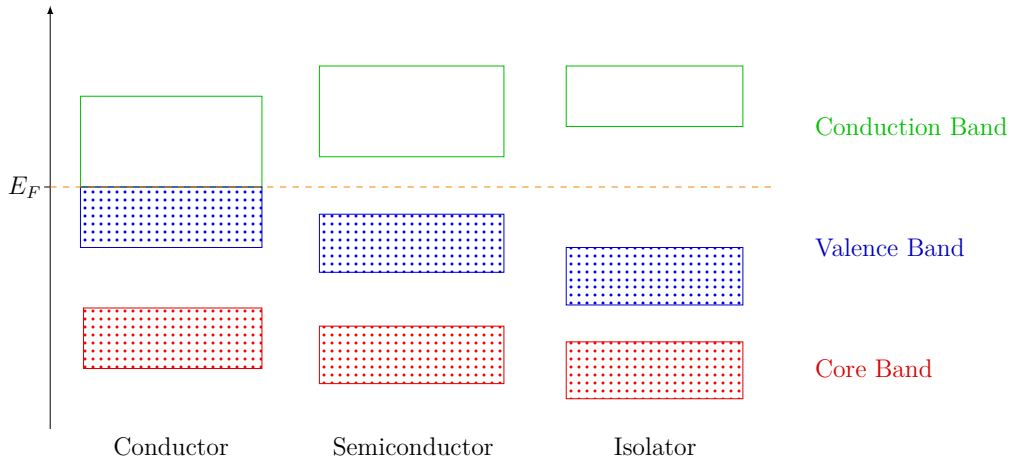

Figure 2: Sketch of the band theory for conductors, semiconductors and isolators. At a temperature of 0 K, the bands lower than the Fermi energy E_F are completely filled, all higher bands are completely empty (full states are marked by dots in the diagram).

2.3 Piezoelectric Effect

The information in this section is taken from [4].

The piezo-effect occurs in piezoelectric materials. When a piezoelectric material is deformed, an electric field is created. The reverse is also true: When a piezoelectric material is exposed to an external electric field, it deforms. The deformation is reversible. This is called the reverse piezo effect and is the one of interest in this experiment. A piezoelectric material is made up of atoms arranged in a way that they create an electric field if they

are exposed to a mechanical force. When such a material is exposed to an external electric field, the atoms rearrange accordingly. This leads to a deformation of the crystal.

2.4 Scanning Tunneling Microscope

The information used in this subsection is taken from the operating instructions included with the STM [5].

In this experiment, a scanning tunneling microscope (STM) is used to image the charge distribution of a structure at atomic level. The scanning tunneling microscope utilizes the phenomenon of quantum tunneling. When a metal tip is held very close (about 10 Å) to a conducting surface and a voltage is applied, the tunneling current caused by electrons tunneling between surface and tip is measurable. However, as given in eq. (4), the measurable current I exponentially decreases with increasing distance between surface and tip. Consequently, the main challenge of imaging is to position the tip at a distance close enough to reach a measurable current without touching the surface. To do so, the piezoelectric effect described in section 2.3 is used to control the positioning of the tip and to move it along the surface. The tip is attached to a piezo-quartz. Electric fields can then be created, deforming the piezo-quartz and thereby moving the tip to its desired position in x, y and z. In a STM, three of these piezo-crystals are used, for the three spacial dimensions.

The measured current, which depends on the position the measurement was taken at, can then be used to draw conclusions about the surface structure of the scanned material. The STM can be operated in two modes. In *Constant Current Mode*, the tunneling current is kept constant by immediately readjusting the height of the tip over the surface when a change in current is measured. The positioning adjustments are then used to determine the surface structure. The other mode is *Constant Height Mode*. In this mode, the tip is moved only parallel to the surface, the height is not adjusted during the measurement. This leads to faster imaging speeds, however, the risk of the tip touching the surface due to an irregular surface structure is increased. In this case, the current measured at different positions is used to determine the surface structure. In general, constant height mode is used when the measuring speed is of interest, e.g. when monitoring a chemical process. When precision is of interest, but speed is not a relevant factor, constant current mode is used.

2.5 Structure of Graphite

Unless specified otherwise, the information in this subsection is taken from [6].

Graphite is made up of different layers of carbon atoms, in which the atoms are structured in a hexagonal lattice.

Inside one of the layers, the electrons can move almost freely, but they can not move between layers. The layers are held together by weak Van der Waals forces.

There are two types of graphite atoms, indicated in this report by α and β. An α-atom of the topmost layer is located directly above another α-atom in the second layer, whereas a β-atom of the topmost layer is located in a hole of the lattice of the second layer. As the distance between the α-atoms is small compared to the β-atoms, the electrons of the α-atoms are bound more tightly to the atoms, leading to a lower energy state. The electrons involved in quantum tunneling are usually those of energies close to the Fermi energy. Therefore, as the STM depends on quantum tunneling, the atoms that mainly can be observed are β-atoms, and the structure observed is triangular (as opposed to hexagonal).

2.6 Structure of Gold

Unless specified otherwise, the information in this subsection is taken from [7].

Gold is a conductor. As described in section 2.2, there is no gap between valence band and conduction band, and conduction band electrons can move freely between atoms. Therefore, electrons are not localized at nuclei, and as they can move freely, the surface charge distribution is mostly uniform. An atomic resolution of gold can not be achieved with a STM. In this experiment, a micro-grid onto which a thin layer of gold is applied is measured. Then, the gold measured has the structure of the grid, which can then be resolved.

2.7 Structure of MoS2

Unless specified otherwise, the information in this subsection is taken from [8].

Molybdenum disulfide (MoS2) is a semiconductor. According to the band theory described in section 2.2 and depicted in fig. 2, the Fermi energy is located in a comparatively small band gap between the valence band and the conduction band. At room temperature, most of the electrons are in the valence band, some are in the conduction band. When a semiconductor is inserted into a STM and a voltage is applied between surface and tip, the resulting image depends on the sign of the voltage. When the voltage at the tip is negative, the electrons tunnel from the tip into the valence band of the semiconductor. When the voltage at the tip is positive, the electrons tunnel from the conduction band of the semiconductor into the tip. As the valence band and the conduction band of MoS2 are made up of different atoms, completely different images are expected for different voltage signs. This makes it possible to distinguish the two atoms.

3 Setup and Execution of the Experiment

First, the graphite sample was attached to the sample holder. To get rid of dust and ensure a surface as even as possible, a piece of tape was used to pull off the uppermost layer of graphite. Next, a tip was manufactured from the platinum iridium wire using wire cutters and pliers. Before doing so, the wire, the wire cutters, the pliers and the sample holder were cleaned with ethanol. As the tunneling current to be measured (described in section 2.1) decreases exponentially with the distance between sample and tip, the end of the tip should optimally be one atom thick. This was attempted by pulling and ripping the wire off rather than cutting it. An optical microscope was used to check the tip. As the thickness of the tip should optimally be one atom, it can not be seen through the microscope. Regardless, it could be checked whether the tip was bent or too flat. If the tip seemed sharp enough, tweezers were used to insert the tip into the scanning tunneling microscope. The sample was inserted in front of the tip and positioned by hand as close as possible to the tip. The clear plastic cover with a lens was put over the tip and sample. The STM was then turned on and the computer software started.

The `Advance` and `Retract` function were used to manually move the sample closer to the tip. This was monitored through the lens by eye, checking the distance of sample to tip by observing the mirrored image of the tip visible in the graphite. It is important to never touch the tip with the sample, as in that case the tip will be destroyed.

The tip voltage was initially set to 1 nA and the current to 54 mV. For the final approach, the STM `Approach` function was activated. When this function is selected, the STM approaches the tip to the sample until the predefined current (here 1 nA) is measured. The imaging is then started automatically. In this experiment, the STM was operated in constant current mode, as this allows the most flexible scanning of any probe.

However, the results were not as expected. When the approach was done and the imaging started, only a black screen could be seen in the topography scans. This means that no current was measured and that the tip was too far away from the sample.

In the attempt to measure an image, a lot of tips were manufactured using various techniques. But even tearing the wire instead of cutting, tearing at various angles, cutting quickly while rotating the wire, rotating the cutter, cutting a little and then tearing the rest, tearing very quickly and every other technique did not result in a picture, in fact, it was not even possible to measure noise.

A big obstacle in the testing of the tips was the STM itself. The `Advance` and `Retract` functions to manually move the sample worked only about 50 % of the time. To combat this, the sample holder was cleaned several times with ethanol. However, this only marginally improved the situation and sometimes the sample had to be adjusted by hand. This also led to larger distances the automatic `Approach` function of the STM had to overcome for the final approach. It was also tried to use shorter tips as it could be observed that the `Advance` and `Retract` functions seemed to work better if the sample was placed farther inside the microscope. To do so, sometimes the rear part of the tip was cut to shorten it.

The automatic `Approach` function for the final approach was also problematic. When it finished approaching, usually an orange light of the `Probe Status` and a black image for the topography scan indicated that the tip was not close enough to the probe. Trying to get an image, the rotation of the tip, the tip voltage, the current at which the approach would be stopped and the approach speed were adjusted in many combinations. The current was varied between 0.5 nA and 2.5 nA the tip voltage between 0.44 mV and 0.84 mV and the rotation between 0° and 360°. However, none of the attempts were successful.

The biggest problem with the `Approach` function was that it often advanced the tip until it was touching the sample. This would usually lead to a completely white image, which was observed numerous times. Additionally, oftentimes the STM would not even recognize that the tip was already in contact with the sample and the approach would not be aborted while it was already obvious that the tip was touching the sample. Every time this happened, a new tip had to be manufactured. Oftentimes, a promising-looking tip could never be tested, as it was immediately driven into the sample and destroyed. This also means that no conclusions could be drawn about what tip-manufacturing-technique was the best, which once again hindered the efforts in learning how to manufacture a good tip.

Sometimes, the `Approach` function would not finish approaching even after more than 30 min. The tip was not in contact with the sample, but the approach would not finish and it was not possible to verify that the tip was approaching the sample at all. When this happened, the approach was manually aborted after some time.

Other attempts to measure something were rotating and replacing the sample. After this was done, all of the steps described above (varying the voltage, current and rotation settings etc.) were repeated. In an attempt to at least measure some noise, the gold sample was also inserted, as, being a conductor, it was thought to be easier to catch a signal from gold. Unfortunately, none of the mentioned attempts were successful. In the end, it was not possible to take even a noisy image of any of the samples.

4 Data Analysis

Despite trying all the techniques described above, we were not able to measure any data. The only scans that could be taken show noise of the tip current, where no topographic data could be acquired. An example is shown in fig. 7a in appendix A. Looking at the fourier transformed image in fig. 7b, it is clearly visible that the measured data contains only noise and no information about the surface, as the frequencies are uniformly distributed over the whole scan area. To perform a sensible analysis after all, older data from another lab team was used to be examined. Unfortunately, nothing more than the filenames is known about the data, so differences in the execution to our own measurement can not be discussed. The used files were called `nach_m_essen.nid`, `nach_m_essen_fein_mittel.nid`, `gold4.nid`, `gold5.nid` and `mos6.nid` for the two graphite samples, the two gold samples and the MoS2 sample, respectively. All further analysis is based on these files. The measurements were not taken by us.

4.1 Examination of the Graphite Sample

In the first part of the experiment, the atomic structure of graphite is examined. The ultimately chosen dataset can be seen in fig. 9. It was taken over a range of 5.1 nm, the tip current was at a set point of 1 nA and the tip voltage at 54 mV. The raw measured image can be seen in fig. 9a. To get clear, evaluable data, the image was post processed using the software `Gwyddion`. First, a leveling by mean plane subtraction was performed, after that the data was leveled, making the facets point upwards. Then, the rows were aligned using the setting `Polynomial` at a degree of 3. Finally, the horizontal scars were corrected. The result can be seen in fig. 9c. To get an even better view, the data was fourier transformed to crop off noise frequencies in the frequency domain. The resulting image in the frequency domain can be seen in fig. 3.

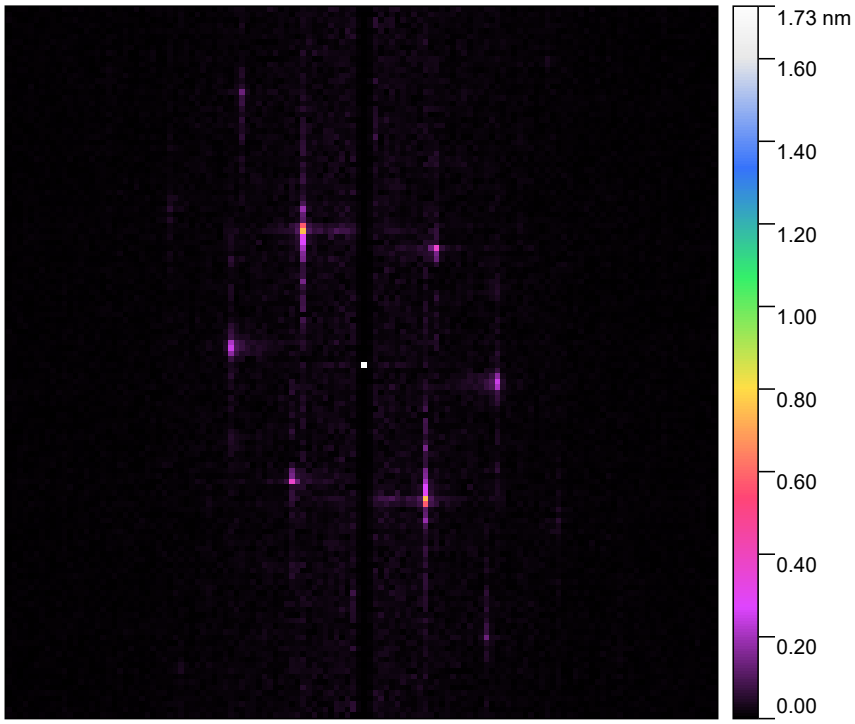

Figure 3: `Old data:` Processed topography scan forward of the graphite sample after a 2-dimensional fourier transformation to the frequency domain. A hexagonal structure surrounded by minor noise is clearly visible. After cropping off the noise and reverse transformation, fig. 4 can be obtained. The original image can be seen in fig. 9a.

A hexagonal structure resulting from the triangular arrangement of the β-atoms of the graphite can be seen. Cropping off the noise around this structure leads to the final image in fig. 4.

Now, a very clear triangular arrangement of the β-atoms is visible and the maximum positions can be examined well.

Before taking a closer look at the positions of the β-atoms, the credibility of this scan needs to be checked. To do so, the forward and backward scan in fig. 9 are compared. Neither the raw output image nor any of the processed images show a major difference in atomic

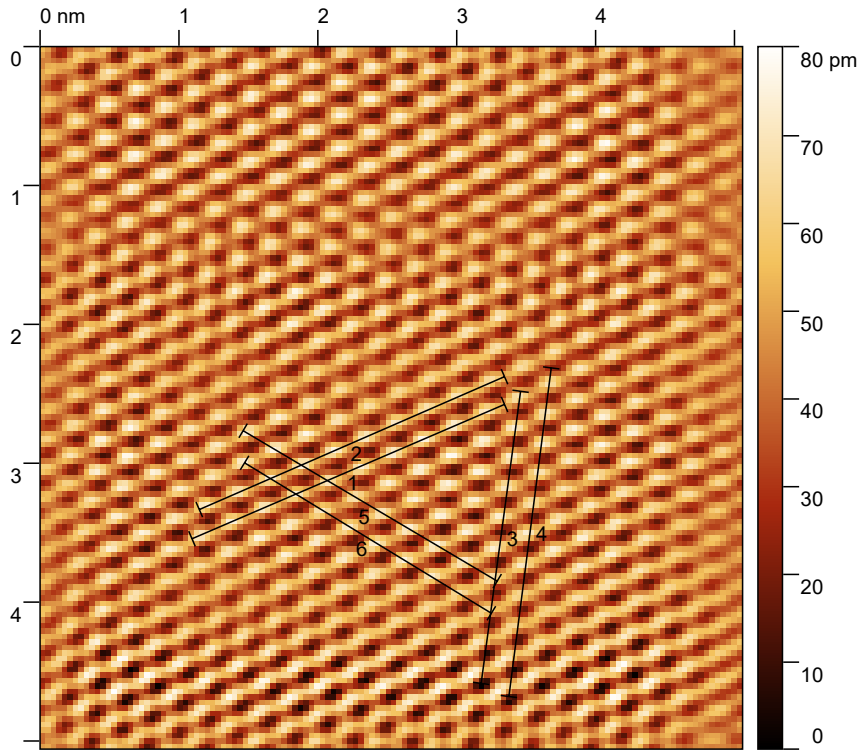

Figure 4: `Old data:` Processed topography scan forward after cropping off noise frequencies in the frequency domain. Now, a very clear triangular structure of maxima can be seen. The lines 1 to 6 were used to create height profiles, visible in fig. 10 to finally calculate the grating constant of graphite. The original image can be found in fig. 9a, a 3-dimensional plot in fig. 11.

structure. As the scans were taken using the same settings, it can be assumed that the images were taken correctly and do not result from major measuring errors. Additionally comparing the close up scans in fig. 9 to the wide range scans in fig. 8 leaves no doubt of the credibility of the data. The triangular graphite structures that are well visible in fig. 9 can also be guessed at there.

To calculate the grating constant of the graphite sample, six height profiles were taken along the lines visible in fig. 4. These height profiles can be seen in fig. 10 in appendix A. The positions of the maxima and their uncertainties were estimated by hand. To calculate the grating constant for each line, the distance between the position x_0 of the first maximum and x_1 of the last maximum was taken and divided by the number n of minima in between. With an uncertainty resulting from gaussian error propagation, the grating constant is calculated to

$$G = \frac{x_1 - x_0}{n} \qquad s_G = \frac{1}{n}\sqrt{{s_{x_0}}^2 + {s_{x_1}}^2}\,. \tag{5}$$

The calculated values for each line are listed in table 1.

Line i	x_0 [nm]	x_1 [nm]	n	G_i [Å]
1	0.07 ± 0.03	2.32 ± 0.02	9	2.50 ± 0.08
2	0.07 ± 0.02	2.28 ± 0.03	9	2.45 ± 0.09
3	0.10 ± 0.02	2.09 ± 0.02	9	2.21 ± 0.12
4	0.11 ± 0.02	2.31 ± 0.02	10	2.20 ± 0.11
5	0.05 ± 0.02	2.10 ± 0.02	9	2.27 ± 0.06
6	0.05 ± 0.02	1.88 ± 0.02	8	2.28 ± 0.07

Table 1: Grating constants of graphite for each line i. The values x_0 and x_1 and their uncertainties were estimated by hand from the height profiles visible in figs. 4 and 10. n is the number of minima along each profile. The grating constant G_i were calculated using eq. (5).

Using these grating constants, an average value can be calculated, using

$$G_{\text{mean}} = \frac{1}{6}\sum_{i=1}^{6} G_i \qquad s_{G_{\text{mean}}} = \sqrt{\frac{1}{5}\sum_{i=1}^{6}\left(G_i - G_{\text{mean}}\right)^2}\,, \tag{6}$$

with the standard deviation as error of G_{mean}. As a final result for the grating constant of the graphite β-atoms, we get

$$G_{\text{graphite}} = (2.32 \pm 0.13)\,\text{Å}\,.$$

4.2 Examination of the Gold Sample

In the second part, a gold sample is examined. It is a micro-grid, covered by a thin film of gold. Therefore, the scan area has to be much bigger than that for the graphite sample. It has been set to 0.2 µm, the tip current was again at a set point of 1 nA and the tip voltage at 54 mV. As before, two different datasets were processed for comparison. They are both visible in figs. 12 and 13. As all four images (samples 1 and 2, scan forward and backward) seem to show a very similar structure after cropping out noise in the frequency domain, there is no reason to suspect an error during the measurement. For the examination of the grating constant of the micro-grid, the backward topography scan of sample two was used. It can be seen in fig. 5.

Here and also especially on the 3-dimensional plot in fig. 15, the structure of the micro-grid can be seen very clearly. To determine its grating constant, again height profiles were used along the lines 1 to 6 shown in fig. 5. All profiles can be seen in fig. 14 in appendix A. As the minima in the height profiles represent the grooves of the grating, the distance between the minima corresponds to the grating constant. To calculate it, the positions of the minima as well as their uncertainties were estimated by hand for each of the six lines. The values can be seen in table 2.

Again, the grating constant was calculated for each line i, using

$$G = x_1 - x_0 \qquad s_G = \sqrt{{x_0}^2 + {x_1}^2}\,. \tag{7}$$

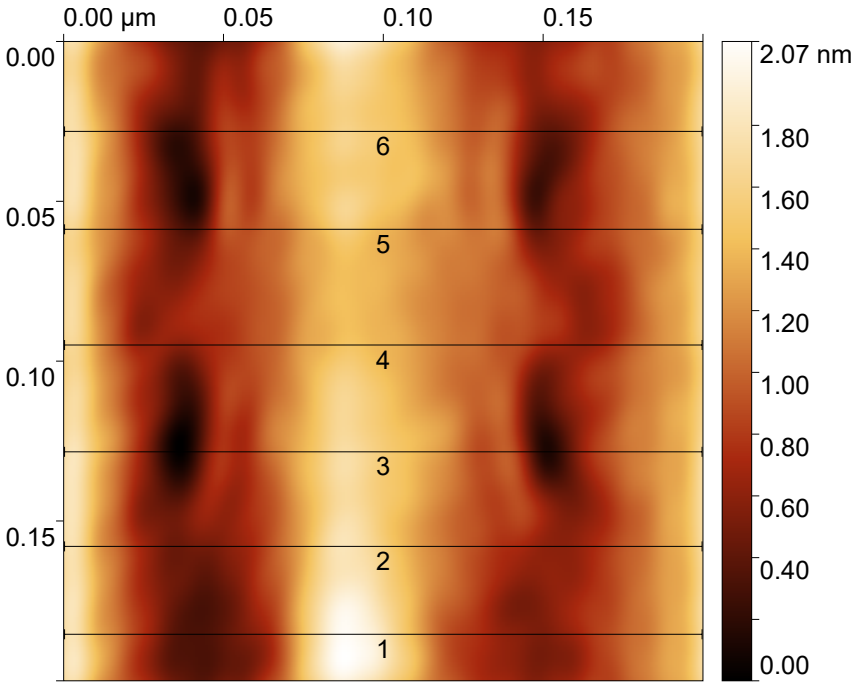

Figure 5: `Old data:` Processed topography scan backward of the gold sample after cropping off noise frequencies in the frequency domain. Now, a very clear segment of the micro-grating can be seen, allowing us to determine the grating constant. The lines 1 to 6 were used to create height profiles, visible in fig. 14, to finally calculate the grating constant using eq. (7). The original image can be found in fig. 13b, a 3-dimensional plot in fig. 15.

Line i	x_0 [nm]	x_1 [nm]	G_i [nm]
1	41 ± 5	149 ± 4	108 ± 6
2	38 ± 6	155 ± 5	117 ± 8
3	36 ± 3	152 ± 3	116 ± 4
4	33 ± 6	162 ± 5	129 ± 8
5	39 ± 4	148 ± 4	109 ± 5
6	35 ± 4	152 ± 4	117 ± 6

Table 2: Grating constants of the gold-covered grating for each line i. The values x_0 and x_1 and their uncertainties were estimated by hand from the height profiles visible in figs. 5 and 14. The grating constant G_i were calculated using the difference in eq. (7).

With eq. (6), the mean value and standard deviation were calculated to be

$$G_{\text{gold}} = (116 \pm 7)\,\mu\text{m}\,.$$

4.3 Examination of the MoS2 Sample

Finally, a MoS2 sample was examined. The objective of this measurement is to differentiate between the two atoms after taking images of the same area with a different tip voltage sign. Unfortunately, in the old datasets, no usable measurement of the MoS2 sample could be found. The only scan is shown in fig. 6.

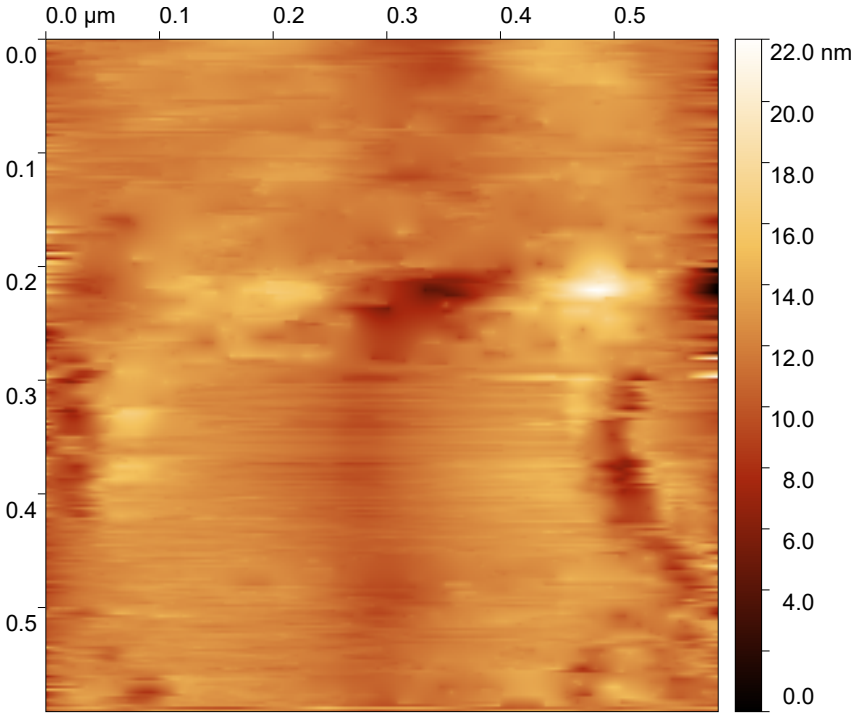

Figure 6: `Old data:` Processed topography scan forward of the MoS2 sample. Unfortunately, no good resolution of any atomic structure can be seen. Therefore, a differentiation between the two atoms is not possible. The original image can be found in fig. 16.

As no atomic structure can be seen, it is not possible to gain any information on the molybdenum and sulfur atoms from this scan. Regardless, it can be said that probably the scan range was set way too big, as the scan shows 0.59 µm on each side. This is clearly a too wide range to see any atomic structures on the sample.

5 Summary and Discussion

As no data could be measured, old data found on the computer was analyzed. With this data, the lattice constant of graphite could be calculated to

$$G_{\text{graphite}} = (2.32 \pm 0.13)\,\text{Å}\,.$$

It is within 2 standard deviations of the literature value of 2.46 Å [1], which means the values are compatible. The relative error of 5.6 % is rather low, which means that the measurements in combination with the post-processing led to a sufficiently clear picture, even though the initially measured pictures seemed rather blurry. It is interesting to see in fig. 4 and table 1 that the calculated grating constants for lines pointing in different directions slightly differ, while they match quite well if the lines are pointing in the same direction. This could result from distortion due to a small rotation of the sample surface with respect to the tip. The measured image of graphite that was used for analysis can be seen in figs. 9a and 9b, and the images after processing in figs. 9e and 9f.

Even though the images of gold were quite blurry, post processing lead to a clear image of the grating. The grating constant of the gold grating was determined to

$$G_{\text{gold}} = (116 \pm 7)\,\mu\text{m}\,.$$

As a literature value is not given, it is not possible to compare the results. However, the calculated value seems to be of reasonable magnitude. The measured image of gold that was used for analysis can be seen in figs. 13a and 13b, and the images after processing figs. 13e and 13f.

Unfortunately, it was not possible to extract any structure from the MoS2-sample data so that an examination of the atomic structure could not be performed.

The main reason no data could personally be taken in this experiment is probably that no good tip was created. However, the scanning tunneling microscope itself was not always working as expected. As described in section 3, the `Advance` and `Approach` functions often did not work. This sometimes made it impossible to test the tips as the scans would not commence due to approaching errors of the microscope.

Also, the conductivity of tip and sample could not be tested. As sometimes the tip was clearly touching the sample, but the scan would not stop, it is also not sure whether there was a problem in connecting the tip well enough to the base or the sample to the sample holder to guarantee a conductivity throughout the measurement. As the scanning tunneling microscope depends on accurate current measurements, a reduced conductivity would have a major impact on the results of the measurement.

Another possible problem is the condition of the samples. Both graphite samples were quite scratched, and taking off the uppermost layer using tape did not lead to a significantly better surface. The gold sample had large scratches as well, and only small regions were usable. Improving the samples might also lead to a better imaging result.

A Appendix

List of Figures

List of Tables

Bibliography

[1] Hugo Strunz; Ernest Nickel, *Strunz Mineralogical Tables. Ninth Edition* (Schweizerbart Science Publishers, Stuttgart, Germany, Dec. 2001), http://www.schweizerbart.de//publications/detail/isbn/9783510651887/Strunz%5C_Hugo%5C_%5C_Nickel%5C_Ernest%5C_H%5C_Strunz.

[2] J. Tersoff and D. R. Hamann, *Theory of the scanning tunneling microscope* (AT&T Bell Laboratories, Murray Hill, New Jersey 07974, 25.06.1984, Sept. 18, 2022).

[3] Wolfgang Demtröder, *Experimentalphysik, Atome, Moleküle und Festkörper* (Springer Spektrum, Sept. 18, 2022).

[4] R. J. Dwayne Miller Ph.D., *Instructional Scanning Tunneling Microscope* (Burleigh Instruments, Inc., Department of Chemistry & the Institute of Optics, University of Rochester, Rochester, NY 14627, Sept. 18, 2022).

[5] *Operating Instructions, easyScan 2 STM, Version 1.6* (NANOSURF AG, SWITZERLAND, PROD.:BT02090, V1.6R0, Sept. 18, 2022).

[6] Sang-II Park and C. F. Quate, *Tunneling microscopy of graphite in air* (Edward L. Ginzton Laboratory, Stanford University, Stanford, California 94305 20.09.1985, Sept. 18, 2022).

[7] V. M. Hallmark, S. Chiang, J. F. Rabolt, J. D. Swalen, and R. J. Wilson, *Observation of Atomic Corrugation on Au(111) by Scanning Tunneling Microscopy* (IBM Almaden Research Center, San Jose, California 95120, 23.07.1987, Sept. 18, 2022).

[8] M. Weimer, J. Kramer, C. Bai, and J. D. Baldeschwieler, *Tunneling microscopy of 2H-MoS_2: A compound semiconductor surface* (California Institute of Technology, Pasadena, California 91125, 08.09.1987, Sept. 18, 2022).

A.1 Our Data

A.1.1 Graphite, close up view

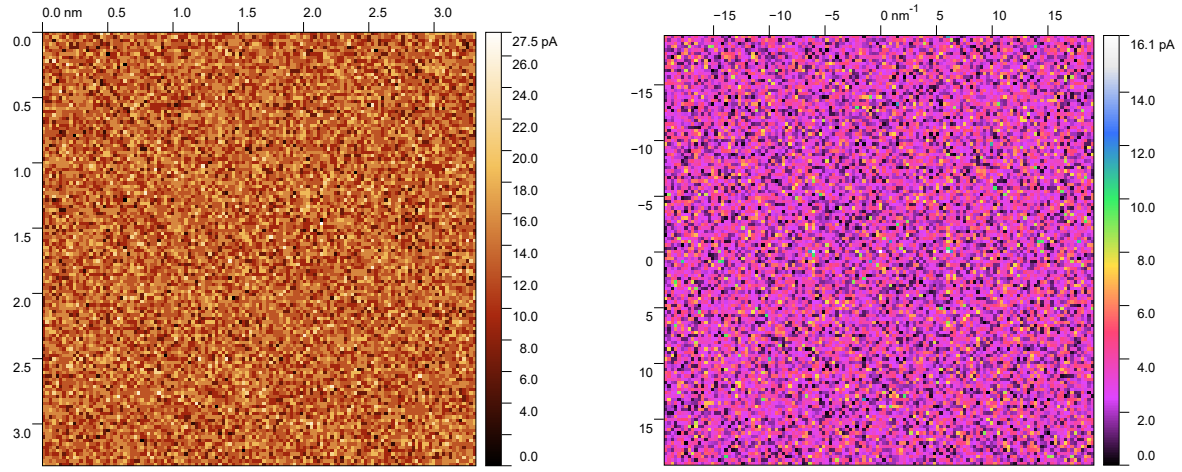

(a) Raw data **(b)** Fourier transformed data

Figure 7: `Our data:` Tip current, scan forward. It can be seen that a huge amount of noise was measured. Also the fourier transformed scan shows no regularities, which proofs that the image contains only noise and no information about the surface. During this measurement, no topography information different from 0 could be taken.

A.2 Old Data

A.2.1 Graphite, wide range view

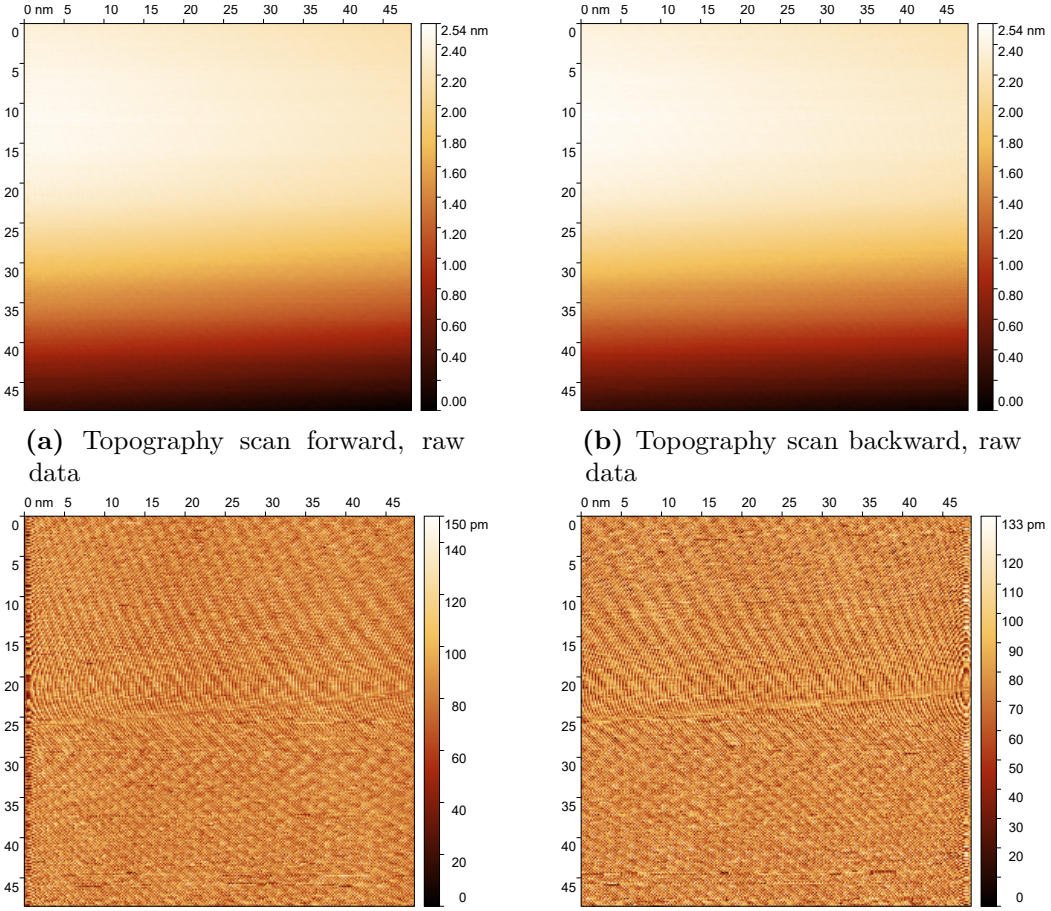

(a) Topography scan forward, raw data

(b) Topography scan backward, raw data

(c) Topography scan forward, processed data

(d) Topography scan backward, processed data

Figure 8: `Old data:` Topography scans of a graphite sample. The image size is 49 nm, taken at a scan rate of 0.8 s per line. Each line contains 256 points and the scan was performed at a rotation angle of 0°. The constant current mode was used, with a tip voltage of 54 mV and a current set point of 1 nA. The forward and backward scans are shown with different filters applied.

A.2.2 Graphite, close up view

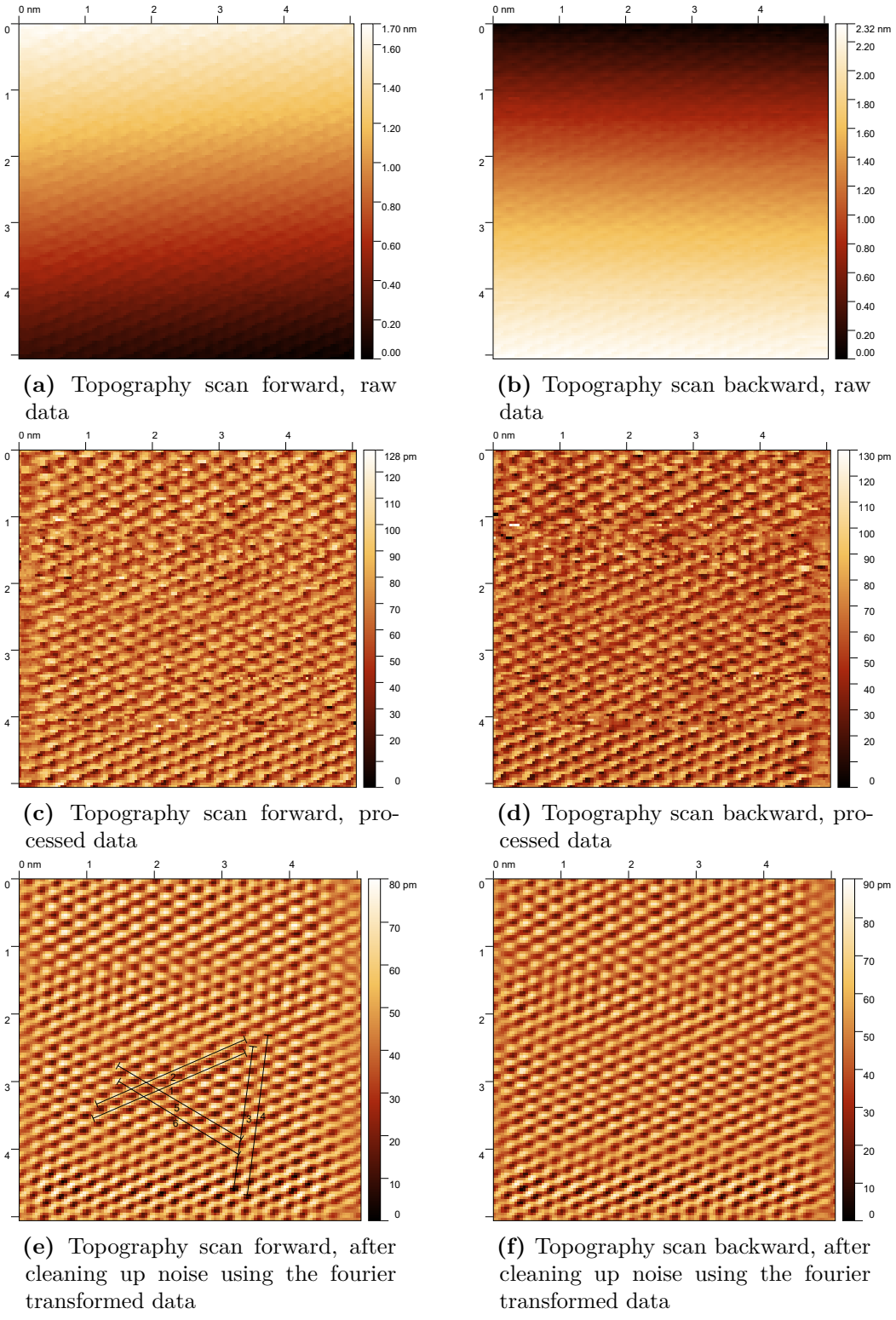

(a) Topography scan forward, raw data

(b) Topography scan backward, raw data

(c) Topography scan forward, processed data

(d) Topography scan backward, processed data

(e) Topography scan forward, after cleaning up noise using the fourier transformed data

(f) Topography scan backward, after cleaning up noise using the fourier transformed data

Figure 9: `Old data:` Topography scans of a graphite sample. The image size is 5.1 nm, taken at a scan rate of 0.4 s per line. Each line contains 128 points and the scan was performed at a rotation angle of 0°. The constant current mode was used, with a tip voltage of 54 mV and a current set point of 1 nA. The forward and backward scans are shown with different filters applied. The final image **(e)** was used for further analysis of the graphite structure.

A.2.3 Graphite, height profiles

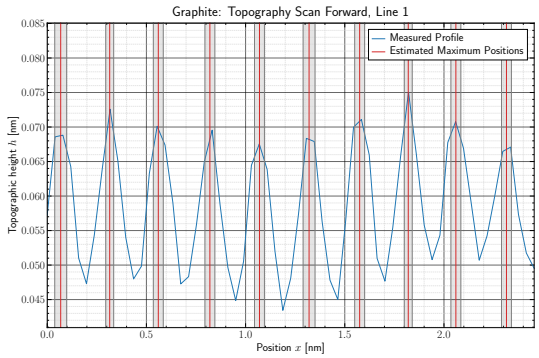

(a) Height profile of line 1

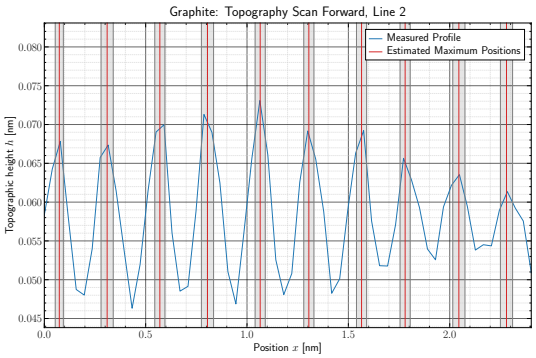

(b) Height profile of line 2

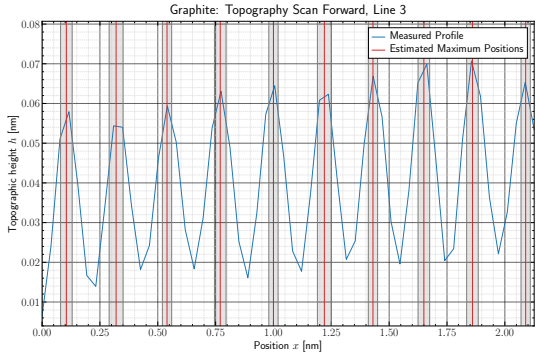

(c) Height profile of line 3

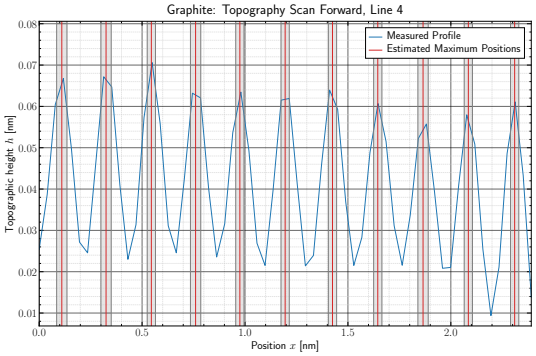

(d) Height profile of line 4

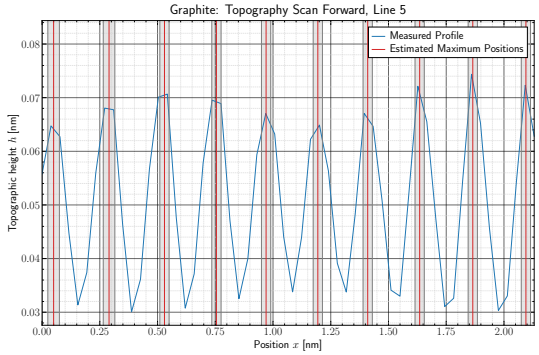

(e) Height profile of line 5

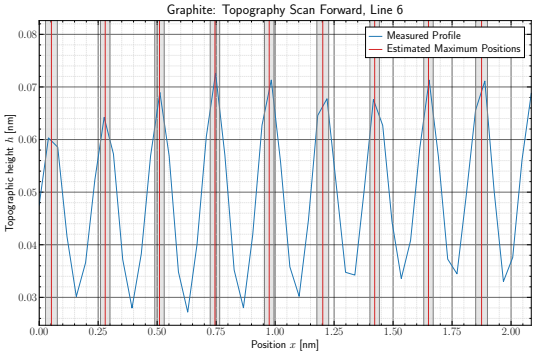

(f) Height profile of line 6

Figure 10: `Old data:` Height profiles of the lines 1 to 6, visible in fig. 4. To get these information, the data was post processed and cleared of noise frequencies in the frequency domain. The maximum positions and their uncertainties were estimated by hand. The resulting values for the distance between the β-atoms can be calculated using eq. (5) and can be found in table 1.

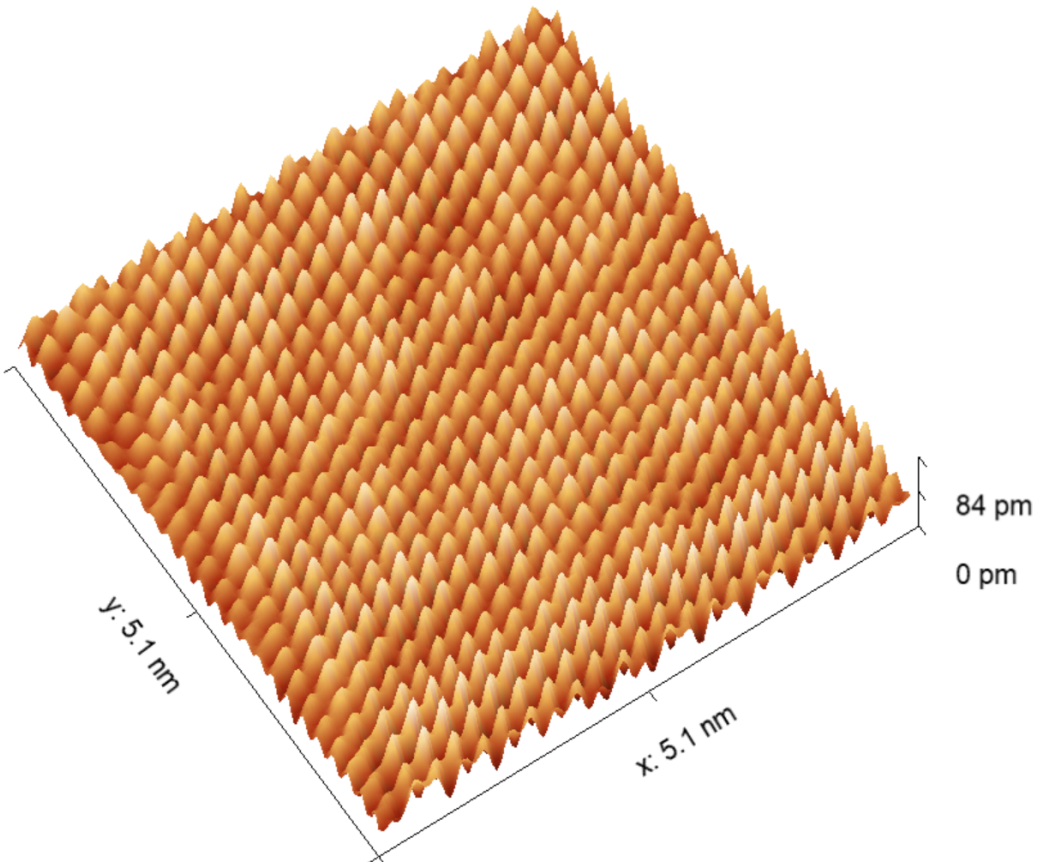

Figure 11: `Old data:` 3-dimensional, processed topography scan forward after cropping off noise frequencies in the frequency domain. A clear triangular structure of maxima can be seen. The original image can be found in fig. 9a.

A.2.4 Gold, sample 1

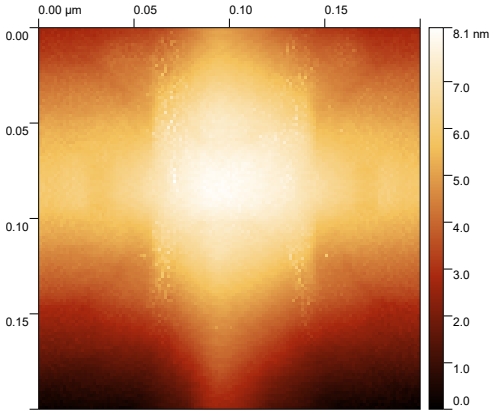

(a) Topography scan forward, raw data

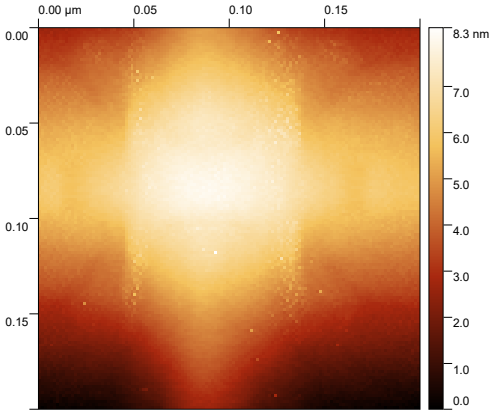

(b) Topography scan backward, raw data

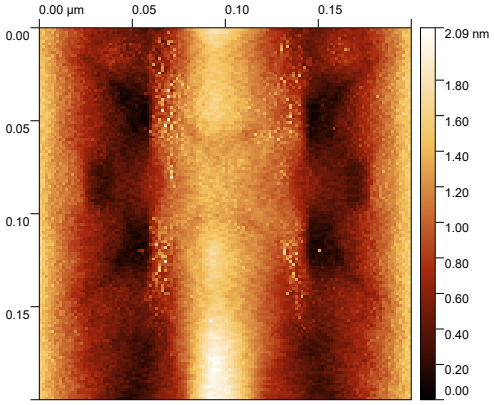

(c) Topography scan forward, processed data

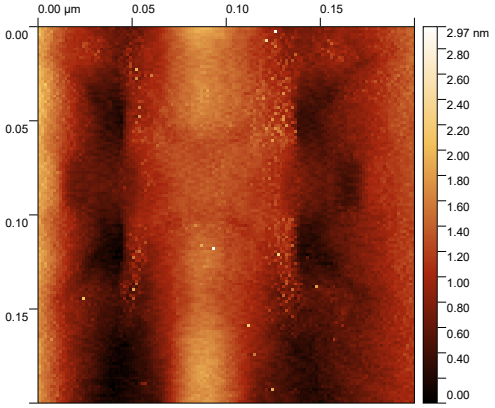

(d) Topography scan backward, processed data

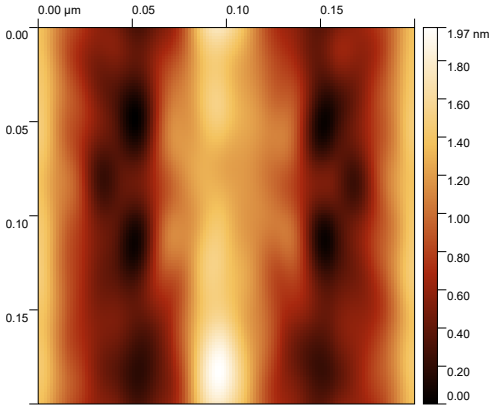

(e) Topography scan forward, after cleaning up noise using the fourier transformed data

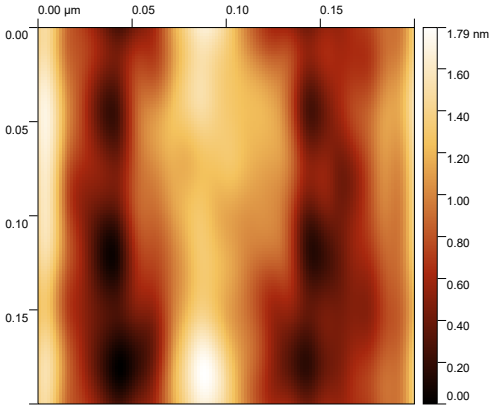

(f) Topography scan backward, after cleaning up noise using the fourier transformed data

Figure 12: `Old data`: Topography scans of the gold sample. The image size is 0.2 µm, taken at a scan rate of 0.8 s per line. Each line contains 256 points and the scan was performed at a rotation angle of 0°. The constant current mode was used, with a tip voltage of 54 mV and a current set point of 1 nA. The forward and backward scans are shown with different filters applied.

A.2.5 Gold, sample 2

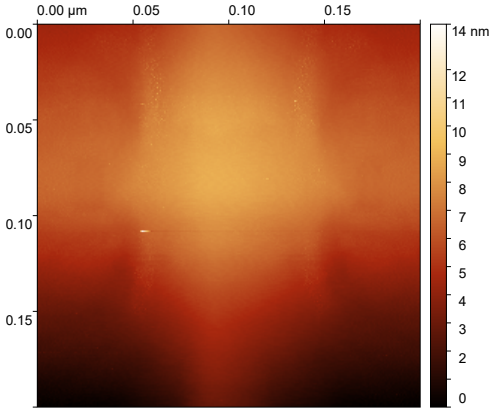

(a) Topography scan forward, raw data

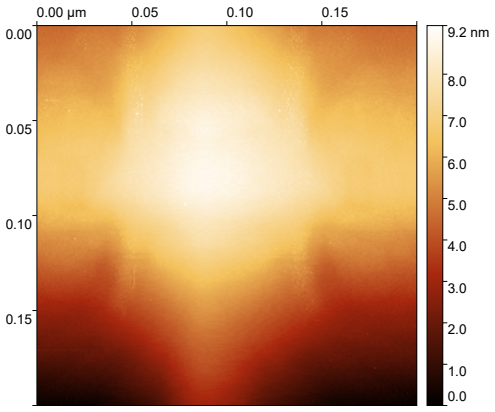

(b) Topography scan backward, raw data

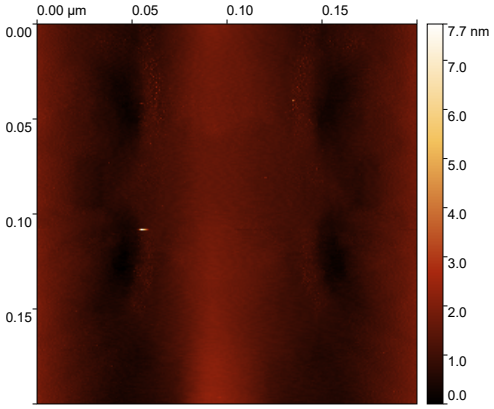

(c) Topography scan forward, processed data

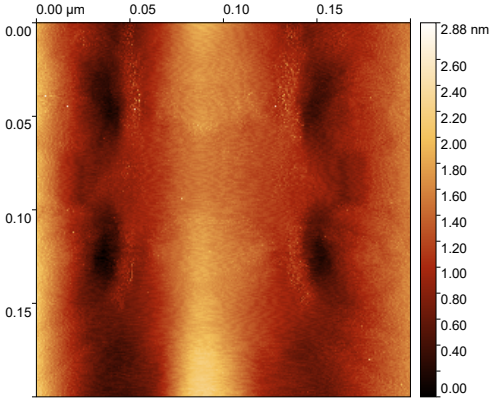

(d) Topography scan backward, processed data

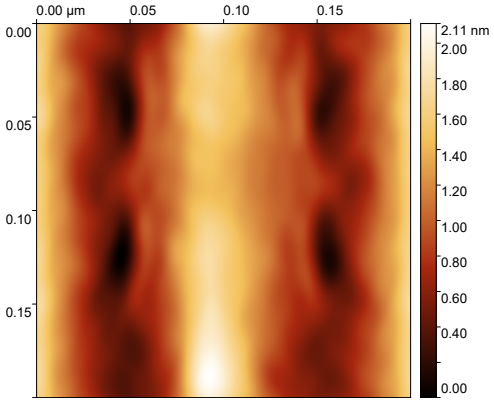

(e) Topography scan forward, after cleaning up noise using the fourier transformed data

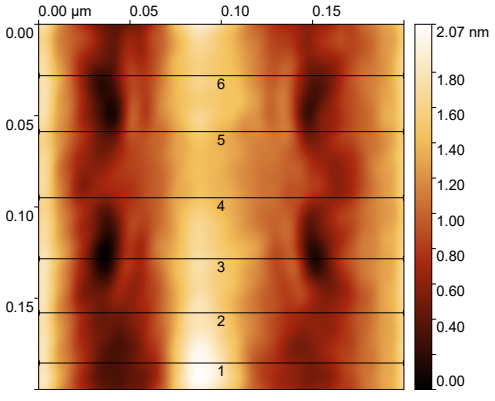

(f) Topography scan backward, after cleaning up noise using the fourier transformed data

Figure 13: `Old data:` Topography scans of the gold sample. The image size is 0.2 µm, taken at a scan rate of 0.8 s per line. Each line contains 256 points and the scan was performed at a rotation angle of 0°. The constant current mode was used, with a tip voltage of 54 mV and a current set point of 1 nA. The forward and backward scans are shown with different filters applied. The final image **(f)** was used for further analysis of the gold-covered micro-grid.

A.2.6 Gold, height profiles

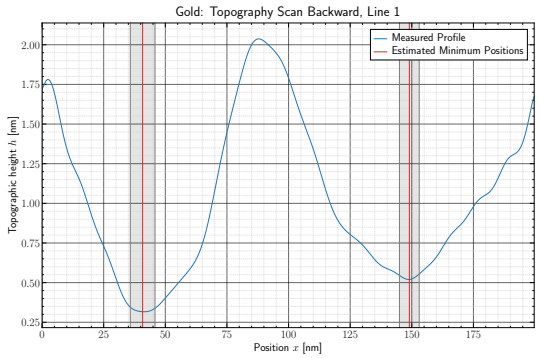

(a) Height profile of line 1

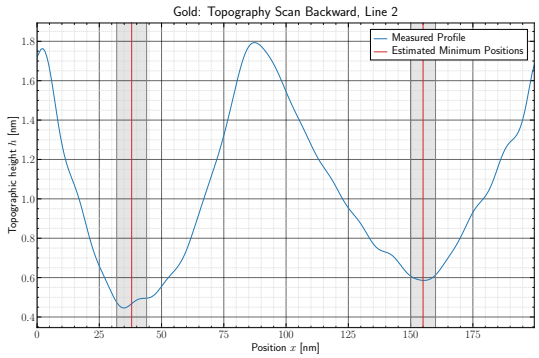

(b) Height profile of line 2

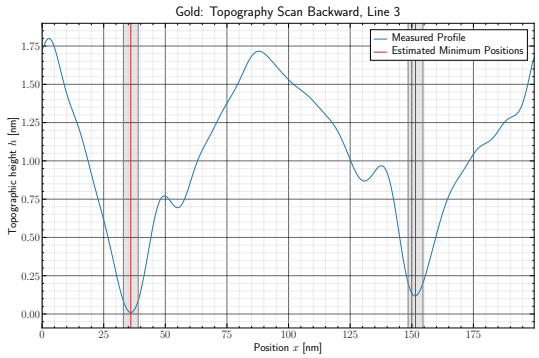

(c) Height profile of line 3

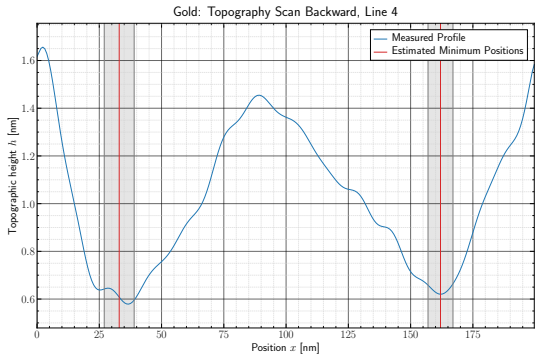

(d) Height profile of line 4

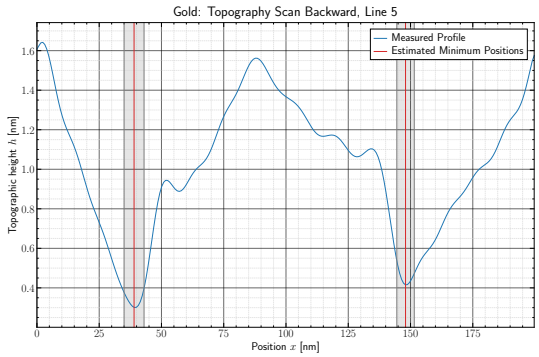

(e) Height profile of line 5

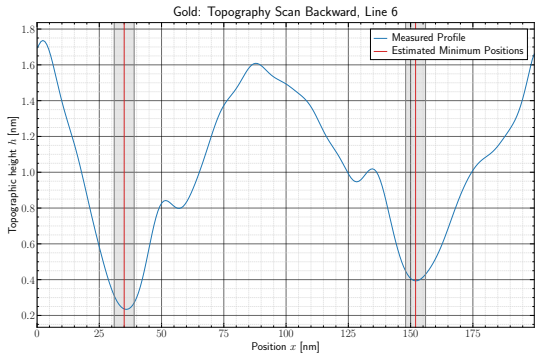

(f) Height profile of line 6

Figure 14: `Old data:` Height profiles of the lines 1 to 6, visible in fig. 5. To get these information, the data was post processed and cleared of noise frequencies in the frequency domain. The minimum positions and their uncertainties were estimated by hand. The resulting values for the grating constant of the micro-grid covered with gold can be calculated by eq. (7) and are shown in table 2.

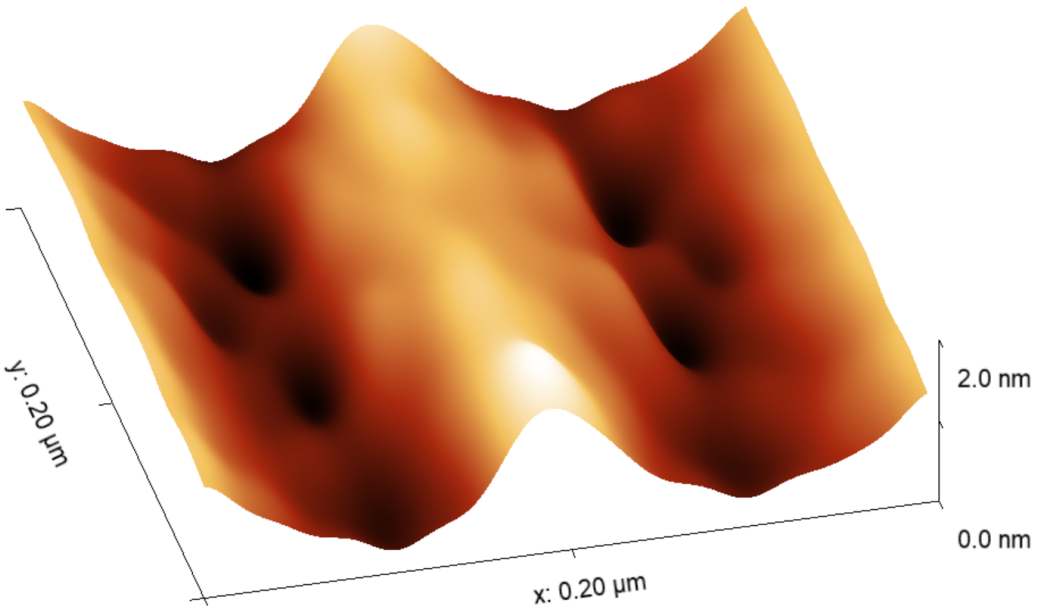

Figure 15: `Old data:` 3-dimensional, processed topography scan backward of the gold sample after cropping off noise frequencies in the frequency domain. A very clear segment of the micro-grid can be seen, allowing us to determine the grating constant. The original image can be found in fig. 13b.

A.2.7 MoS2, wide range view

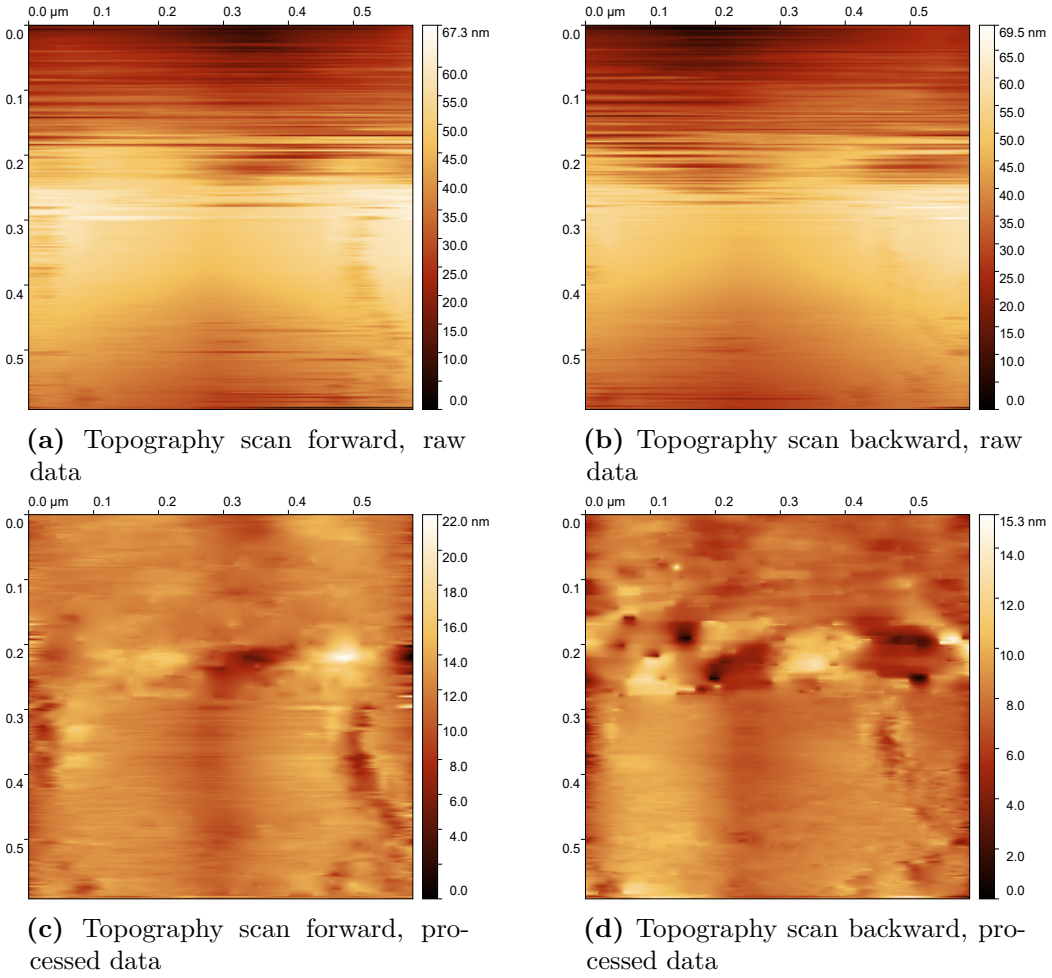

(a) Topography scan forward, raw data

(b) Topography scan backward, raw data

(c) Topography scan forward, processed data

(d) Topography scan backward, processed data

Figure 16: `Old data:` Topography scans of a MoS2 sample. The image size is 0.59 µm, taken at a scan rate of 0.8 s per line. Each line contains 256 points and the scan was performed at a rotation angle of 0°. The constant current mode was used, with a tip voltage of −54 mV and a current set point of −1 nA. The forward and backward scans are shown with the raw data and after processing.

A.3 Lab Notes

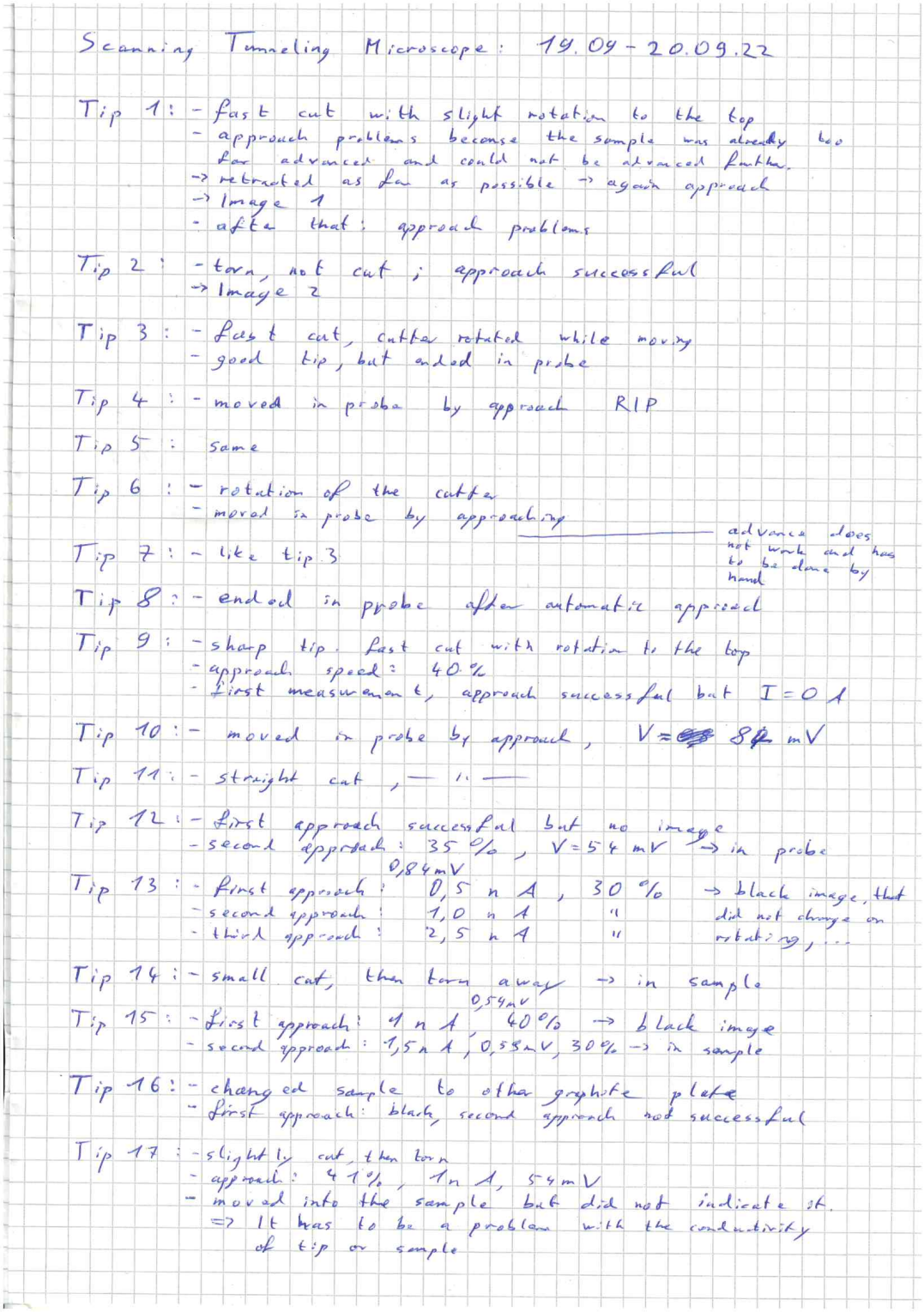

Scanning Tunneling Microscope: 19.09 - 20.09.22

Tip 1: - fast cut with slight rotation to the top
- approach problems because the sample was already too far advanced and could not be advanced further.
→ retracted as far as possible → again approach
→ Image 1
- after that: approach problems

Tip 2: - torn, not cut; approach successful
→ Image 2

Tip 3: - fast cut, cutter rotated while moving
- good tip, but ended in probe

Tip 4: - moved in probe by approach RIP

Tip 5: same

Tip 6: - rotation of the cutter
- moved in probe by approaching

Tip 7: - like tip 3 — advance does not work and has to be done by hand

Tip 8: - ended in probe after automatic approach

Tip 9: - sharp tip, fast cut with rotation to the top
- approach speed: 40 %
- first measurement, approach successful but I = 0 A

Tip 10: - moved in probe by approach, V = 84 mV

Tip 11: - straight cut, — " —

Tip 12: - first approach successful but no image
- second approach: 35 %, V = 54 mV → in probe
0,84 mV

Tip 13: - first approach: 0,5 n A, 30 % → black image, that
- second approach: 1,0 n A " did not change on
- third approach: 2,5 n A " rotating, ...

Tip 14: - small cut, then torn away → in sample
0,54 mV

Tip 15: - first approach: 1 n A, 40 % → black image
- second approach: 1,5 n A, 0,58 mV, 30 % → in sample

Tip 16: - changed sample to other graphite plate
- first approach: black, second approach not successful

Tip 17: - slightly cut, then torn
- approach: 41 %, 1 n A, 54 mV
- moved into the sample but did not indicate it.
=> It has to be a problem with the conductivity of tip or sample

Tip 18: sample = gold, tip in sample after approach problems, advance + retract did not work

Tip 19: first approach: only black screen
second approach: — " —
waited for 5 rescans, adjusted rotation, slope, ...

Tip 20: used graphite again, 1 successful approach, still black

Tip 21: in sample during approach

Tip 22: no measurement possible

Tip 23; 24, 25, 26, 27, 28, 29 varying tip voltage from 0,54V-0,68V

Tip 30: will not approach for $I = 1{,}5$ nA, $V = 54$ mV
→ in sample

F. Müller